Dry reforming of methane in a temperature-controlled dielectric barrier discharge reactor: disclosure of reactant effect

Xuming Zhang[1]*, Yesheng Wenren[1], Weili Zhou[2], Jingyi Han[2], Hao Lu[2*], Zuchao Zhu[1], Zuliang Wu[2*], Suk Cha[3]

E-mail address: miraclezhang918@163.com (X. Zhang), luhaozju@163.com (H. Lu)

1. State-Province Joint Engineering Lab of Fluid Transmission System Technology, Zhejiang Sci-Tech University, Hangzhou, Zhejiang 310018, China
2. School of Environmental Science and Engineering, Zhejiang Gongshang University, Hangzhou, Zhejiang 310018, China.
3. King Abdullah University of Science and Technology (KAUST), Clean Combustion Research Center (CCRC), Physical Science and Engineering Division (PSE), Thuwal 23955, Saudi Arabia

Abstract: Plasma-assisted dry reforming of methane has attracted much research attention because this process simultaneously utilizes greenhouse, methane and carbon dioxide, to produce hydrogen-rich syngas at a relative low temperature. Although it is generally recognized that the gas composition of reactant has great effect on the methane conversion and products distribution, systematic studies that clarify the roles that electron-induced chemistry and thermochemistry play are needed for a full understanding of reactant effect. Here, we compared the reforming performance by varying the ratio of CO_2/CH_4 or O_2/CH_4 at the similar reduced field intensity (*E/N*) in a temperature-controlled dielectric barrier discharge reactor to elaborate the role of electron-induced chemistry and thermo-chemistry in the dry reforming process. By conducting optical emission spectrum measurement, the enrichment of O atoms was observed at the increased CO_2/CH_4 or O_2/CH_4 ratios. At $T = 293$ K, methane conversion was only dependent on the electron-induced chemistry regardless of the specific reactant gas composition. At a relative high temperature condition, however, thermochemistry could become pronounce when sufficient O atoms were added into the dry reforming process. In contrast, the chemical pathways to the products were overall controlled by the thermochemistry at the tested background temperatures. Due to the conversion of carbon-based products into the carbon dioxide, the conversion of carbon dioxide was influenced by the thermochemistry when the concentration of O atoms was high. Our findings may improve the understanding of reactant effect and the designs of plasma-reformer.

Key Words: dry reforming, plasma, carbon dioxide, methane, gas composition

1. Introduction

Today, under the pressure of serious environmental problems caused by the excessive use of fossil fuels, the demand for renewable and environmental-friendly energy is becoming ever more urgent. The reforming (or gasification) of conventional feedstock as fuel, of which major constituent is carbon and hydrogen, for the production of hydrogen-rich syngas or value-added chemicals has showed promising potential. Various reforming methods, such as partial oxidation, steam reforming, and dry reforming, are designed mainly to produce hydrogen and carbon monoxide and yield typical H_2/CO ratio with each reforming process. Among these reforming processes, the dry reforming of methane, a reaction between methane (CH_4) and carbon dioxide (CO_2), has attracted much research attention because this process simultaneously utilizes and reduces greenhouse [1]. Catalytic processes for the dry reforming are limited by rapid deactivation of the catalysts due to coke formation. Moreover, a requirement of warm-up period to reach activation temperatures also limits the catalytic process in some applications, e.g. in vehicles, which require rapid ignition/start-up from a cold condition. In this reason, studies based on non-thermal plasma (NTP) techniques have been conducted to fill the technical gap [2−5].

Different NTP generation methods [6−10] as well as the combinations of NTP with heterogeneous catalysts [11−16] have been investigated to make the process commercially feasible in terms of energy efficiency and product selectivity. It is generally recognized that the *hotter* plasmas, e.g. arc-jet type plasma and microwave plasma, are superior to the *colder* plasmas, which are typically produced by dielectric barrier discharge (DBD) and corona discharge, in the CH_4 and CO_2 conversion, and H_2 selectivity [17−21]. The advantage of the *colder* plasmas is its low temperature, so it is possibly to obtain useful chemical intermediates that do not reach deep oxidation (CO_2) or cracking (soot) [22−26].

The improvement of the reactant conversion and products distribution using the *colder* plasmas requires a better understanding of plasma chemistry in the reforming process. In previous work, we developed a temperature-controlled DBD reactor. This reactor allows individually controlling the reduced filed intensity and reaction

temperature, which govern the electron-induced chemistry and thermochemistry, respectively. As a result, we found that for the dry reforming of CH_4 at CO_2/CH_4=1, the CH_4 conversion was influenced by the electron-induced chemistry while for the partial oxidation of CH_4, the CH_4 conversion was governed by both the electron-induced chemistry and the thermochemistry. However, for both of these reforming processes, the reaction pathways to the products were only affected by the thermochemistry [27, 28]. These results indicate that the plasma chemistry involved in the reforming process could be adjusted by the reactant gas composition. In this regard, the reactant gas composition effect needs to be further investigated so that we can get a deeper understanding of the contribution of electron-induced chemistry and thermochemistry to the CH_4 conversion and products distribution.

In the present study, we systematically investigated the effect of reactant gas composition on the dry reforming of CH_4 with the temperature-controlled DBD reactor. The reactant conversion and products selectivities with the different reactant gas compositions were compared at the similar reduced field intensity and background temperature. The performance was evaluated in terms of CH_4 and CO_2 conversions and product selectivity. The role of electron-induced chemistry and thermochemistry in the reforming process was discussed on the basis of the results of performance elevation, optical emission spectroscopy and BOLSIG+ based numerical calculation

2. Experimental setup

Figure 1 shows the schematic of the setup for the experiment. The experimental setup consisted of a temperature-controlled DBD reactor, a high-voltage supplier, a reactant feeding system, and a measurement system. Similar configuration was used in our previous work [27, 28]. The temperature-controlled DBD reactor includes a coaxial DBD reactor and an electric oven. The coaxial DBD was constructed of a quartz tube with a length of 200 mm and an inner diameter of 20.0 mm, which was used as a dielectric barrier. The outer wall of the quartz tube was wrapped with 45-mm-wide stainless-steel mesh, which was used as a grounding electrode. A stainless-steel rod with a diameter of 17.5 mm was inserted into the quartz tube to serve as a high-voltage electrode. The resulted discharge gap was ~1.3 mm.

An amplifier (20/30 A, Trek) in conjunction with a function generator (AFG 3021B,

Tektronix) was used to generate AC high voltage. The AC high voltage and discharge current were measured by a digital oscilloscope (DPO 4140B, Tektronix) together with a high voltage probe (P 6015A, Tektronix) and a current monitor (6595, Pearson), respectively. The typical value of V_{peak}/V_{rms} was 1.6. *V-Q* Lissajous method was used to determine the discharge power into the DBD reactor. The charge *Q* was calculated by measuring a voltage across a 30 nF capacitor, using a voltage probe (TPP 1000, Tektronix). The *V-Q* Lissajous diagram was averaged over 216 scans, and the discharge power was calculated from the area of the diagram by multiplying the frequency. Optical emission spectroscopy (OES) was conduced by a spectrometer (Acton SP2500i, Princeton Instruments) equipped with a slit (100 μm), a grating (600 grooves mm^{-1}) and a highly sensitive camera (PIXIS-100, Princeton Instruments) with the exposure time of 100 ms.

The flow rate of each component was controlled by a mass flow controller (MFC) (SLA5850, Brooks Instrument). The total flow rate was fixed at 200 ml/min. An electric oven (O series, NDB Co. Ltd.) was used to heat the gas mixture to a target temperature. A homemade ice-water-cooling trap was used to condense liquid products. The feed and product gas were analyzed using an online gas chromatograph (HP 7890A, Agilent) equipped with a flame ionization detector (FID) and two thermal conductivity detectors (TCD).

To characterize the dry reforming process, the CH_4 and CO_2 conversions were defined as:

$$CH_4 \text{ conversion}(\%) = \frac{\text{moles of } CH_4 \text{ converted}}{\text{moles of } CH_4 \text{ input}} \times 100 \quad \text{(E1)}$$

$$CO_2 \text{ conversion}(\%) = \frac{\text{moles of } CO_2 \text{ converted}}{\text{moles of } CO_2 \text{ input}} \times 100 \quad \text{(E2)}$$

The selectivities of the products were calculated as:

$$H_2 \text{ selectivity}(\%) = \frac{\text{moles of } H_2 \text{ produced}}{2\times \text{ moles of } CH_4 \text{ converted}} \times 100 \quad \text{(E3)}$$

$$\text{CO selectivity}(\%) = \frac{\text{moles of CO produced}}{\text{moles of } CH_4 \text{ converted} + \text{moles of } CO_2 \text{ converted}} \times 100 \qquad \text{(E4)}$$

$$C_XH_Y \text{ selectivity}(\%) = \frac{X \times \text{moles of } C_XH_Y \text{ produced}}{\text{moles of } CH_4 \text{ converted} + \text{moles of } CO_2 \text{ converted}} \times 100 \qquad \text{(E5)}$$

and the H_2/CO molar ratio was defined as:

$$\frac{H_2}{CO} = \frac{\text{moles of } H_2 \text{ produced}}{\text{moles of CO produced}} \qquad \text{(E6)}$$

3. Results

3.1. DBD characteristics

Since varying background temperature or reactant gas compositions might affect plasma physics, we investigated the discharge characteristics of the DBD for all experimental conditions. Typical voltage-current waveform and Lissajous diagrams are shown in the Fig. S1 and Fig. S2 of the Supporting Information. In generally, the responses of the lissajous diagrams to the background temperatures for the different reactant gas compositions were similar to that for the dry reforming [28] and partial oxidation process [27]. At T ≤ 673 K, the lissajous diagram showed a sharp parallelogram shape. The discharge pattern from the DBD with a mixture of $CH_4/CO_2/N_2$ at $T \leq 673$ K appears to be in the typical filamentary micro-discharge mode [29] of DBD. At T=773 K, however, the diagram changes from a sharp parallelogram shape into a smooth shape. This change is due to the significant reduction in the resistances of the gas gap and the barrier [28]. Because of these significant resistances' reduction, the discharge mode at 773 K can be characterized as the co-existence of micro-discharges and resistive waste of electrical power [28]. Thus, in this study, the maximum background temperature was set at 673 K.

In the present study, the reduced field intensity (E/N) was varied by the background temperature. The E/N value was estimated by $E/N \approx U_b/(dN)$, where E is the averaged electric field, N is the gas number density, d is the gas gap distance, and U_b is the breakdown voltage in the gas gap. U_b could be calculated from $U_b = U_{on}/(1 + C_g/C_d)$, where U_{on} is the onset voltage, C_d is the effective capacitances of the dielectric barrier, and C_g is the effective capacitances of the gas gap which can be calculated via C_g =

$C_dC_{tot}/(C_d - C_{tot})$, where C_{tot} is the effective capacitance of the total system. Among these values, U_{on}, C_d, and C_{tot} could be determined from the lissajous diagrams based on the well-developed DBD model [30]. Table 1 summarizes the estimated *E/N* values for all tested conditions. As shown in the Table 1, the *E/N* value was more sensitive to the background temperature than to the reactant gas compositions.

In addition, we investigated the optical emission spectra of the DBD for the different reactant gas compositions. Each spectrum was normalized with the measured light intensity of the N_2 (C−B) emission band that peaked at 380.3 nm. As shown in Fig. 2a, the emission spectrum of the DBD dry reforming was dominated by the emission of N_2* related bands, such as N_2 C−B and N_2^+ B−X. The CH bands peaked at 431.4 nm and C_2 swan peaked at 516.5 nm were also observed indicating the electron dissociation of the CH_4. As compared to the condition of CO_2/CH_4=1, an atomic line peaked at 777.1 nm was appeared in the condition of CO_2/CH_4=4 indicating the enrichment of the O atoms (Fig. 2b). When O_2 was added into the dry reforming process (Fig. 2c), the bands of CH were reduced by half (as compared to the condition of CO_2/CH_4=1) and the bands of C_2 swan disappeared, while the O atom line also appeared.

3.2. Reforming at room temperature

3.2.1. The effect of CO_2/CH_4 ratio on the dry reforming

Figure 3 shows the effect of CO_2/CH_4 ratio on the dry reforming of CH_4 at T=293 K and fixed discharge power (P_{dis}=10 W). When CO_2/CH_4 ratio was increased from 0.5 to 4, the conversions of CH_4 and CO_2 were kept at around 7.5 % and 3.3% (Fig.3a), respectively. Although the ratio of CO_2/CH_4 did not significantly affect the CH_4 and CO_2 conversion, it obviously altered the product distribution; the selectivities of H_2, C_2H_6, C_2H_4, C_3H_8, and other HCs (Fig.3b) were decreased from 46.8 to 40.2 %, 21.4 to 3.1%, 0.9 to 0.1, 1.8 to 0.2 and 0.8 to 0.1, respectively, while the selectivity of CO increased from 58.7 to 75.9%. It is worth mentioning that the production of CO was mainly attributed to the decomposition of CO_2, because the amount of produced CO was linearly dependent on the conversion of CO_2 as shown in the Supporting Information of Fig. S3. However, carbons would be more or less produced from the dry

reforming process and deposited on the DBD reactor. When the concentration of O atom is high, these carbons are possible oxidized into the CO which might be responsible for the abrupt change in the CO selectivity at a relative high CO_2/CH_4 (CO_2/CH_4=1.5) condition. In addition, due to the varied H_2 and CO selectivity the ratio of H_2/CO decreased from 2.1 to 0.4.

3.2.2. The effect of O_2 addition on the dry reforming

Figure 4 shows the effect of O_2 percentage on the dry reforming of CH_4 at CH_4/CO_2=1, T=293 K, and P_{dis}=10 W. The addition of O_2 did not affect the CH_4 conversion but obviously influenced the CO_2 conversion and O_2 conversion; when increasing O_2/CH_4 from 0.2 to 0.8, the conversion of CH_4 was kept at around 8.2%, but the conversion of CO_2 and O_2 decreased from 2.8 to 1.3% and 55.7 to 12.7% respectively (Fig. 4a). Regarding the products (Fig. 4b), the selectivity towards H_2, C_2H_6, C_2H_4, C_3H_8 and other HCs decreased from 44.4 to 16.2%, 13.3 to 1.7%, 0.3 to 0.06%, 0.8 to 0.04%, 0.4 to 0.02%, respectively, while the selectivity towards CO increased from 59.4 to 84.6%, and the ratio of H_2/CO decreased from 1.0 to 0.3. It seems that the response of products distribution to the varying O_2/CH_4 were much significant than that to the varying CO_2/CH_4. In addition, when O_2 was added into the dry reforming process, the production of CO was not due only to the conversion of CO_2, because the selectivity of CO was even increased with the decrease of CO_2 conversion.

3.3. Dry reforming at a relative high temperature

Figure 5 shows the CH_4 and CO_2 conversion, and products selectivities with different CO_2/CH_4 ratios at T=493 K and P_{dis}=10 W. Unlike the CH_4 conversion at room temperature (T=293 K), the CH_4 conversion at T=473 K was increased (7.7 to 10.3%) with the increase of CO_2/CH_4 ratio (0.5 to 4). In contrast, the response of CO_2, H_2, HCs and CO to the CO_2/CH_4 ratio *at* T=493 K was similar to these at T=293 K; when increasing CO_2/CH_4 ratio from 0.5 to 4, the conversion of CO_2 did not significantly change, while the selectivities of H_2 and HCs decreased, and the selectivity of CO increased as shown in Fig. 5. These results indicate that the reaction pathways of CO_2 conversion and products formation was not significantly changed with the CO_2/CH_4 ratio at higher background temperature condition.

The increase in O_2/CH_4 ratio (CO_2/CH_4=1) led to the obvious increase of CH_4 conversion at T=473 K (Fig. 6). In addition, as compared to the condition at T=293 K, the CO_2 conversion, and H_2, CO and HCs selectivity seem more sensitive to the O_2/CH_4 ratio at T= 473 K, because these values changed more significantly with the O_2/CH_4 ratio at T=473 K than those with the O_2/CH_4 ratio at T=293 K.

3.4. Effect of reduced field intensity on dry reforming

Figure 7 shows the effect of reduced field intensity (E/N) on CH_4 conversion, CO_2 conversion and products selectivities with different reactant gas compositions at fixed discharge power (P_{dis}=10 W). When adding O_2 into the dry reforming process, the CO_2/CH_4 value was kept to be 1. The E/N value was modified by varying the background temperature. It should be noted that the maximum E/N value was limited to ~165 Td, because the background temperature was controlled less than 673 K by considering the DBD mode [28]. The results of the dry reforming at 673 K were abstracted from our previous work [22, 28].

As shown in Fig. 7a, when the E/N was increased from 70 to 160 Td, the CH_4 conversion increased from 7.8 to 11.5% for CO_2/CH_4=1. At the E/N value between 70 to 80 Td (corresponding to T=293 K), no obvious difference was observed between different reactant gas compositions. At the higher E/N value, however, the CH_4 decreased in the order of O_2/CH_4=0.8 >> CO_2/CH_4=4 > CO_2/CH_4=1 at the comparable E/N value. Regarding to the CO_2 conversion (Fig. 7b), at the comparable E/N value, the CO_2 conversion decreased in the order of CO_2/CH_4=1 ≈ CO_2/CH_4=4 > O_2/CH_4=0.8 at $E/N \leq 120$ Td, while it decreased in the order of CO_2/CH_4=1 > CO_2/CH_4=4 > O_2/CH_4=0.8 at E/N > 120 Td.

As for the products, the selectivity of H_2 decreased with the increase of E/N value (Fig. 8a), and it decreased in the order of CO_2/CH_4=1 > CO_2/CH_4=4 > O_2/CH_4=0.8 regardless of the specific E/N value. However, the selectivity of CO increased with the E/N value for the O_2/CH_4=0.8 (Fig. 8b), while it decreased with the E/N value for the CO_2/CH_4=1 and CO_2/CH_4=4. It decreased in the order of O_2/CH_4=0.8 > CO_2/CH_4=4 > CO_2/CH_4=1. Thus, the H_2/CO value could be varied in a wide range (Fig. 8d). In contrast to the trend of the selectivity of CO, the selectivity of HCs decreased with the

E/N value for the O_2/CH_4=0.8 (Fig. 8d), while it increased with the *E/N* value for the CO_2/CH_4=1 and CO_2/CH_4=4.

4. Discussion

We have shown that the variation of the reactant gas composition affected CH_4 and CO_2 conversion, and products distribution. This should be possibly attributed to the modified electron-induced chemistry or the thermochemistry by the change of the reactant. Table 2 summarized important reactions that are responsible for the plasma-assisted dry reforming with the tested reactant gas compositions [31−33]. At a low temperature condition, the plasma-assisted dry reforming process is initialed by the electron-impact dissociation reactions rather than thermal decomposition. The efficiencies of these dissociation reactions depend on electron density and electron energy, which are respectively determined by the energy density and the reduced field intensity (*E/N*) [27, 28].

A calculation from BOLSIG+ software [34] (Fig. S4 of the Supporting Information) indicated that, in the tested *E/N* value range, the reaction (R1) is responsible for ~83% of the total electron dissociation of CH_4, while reactions (R2) and (R3) are responsible for ~13% and ~3%, respectively. It is worth mentioning that the contribution of the reactions between metastable N_2^* and CH_4 could not be ignore due to the high concentration of the metastable N_2^* in the reforming process (Fig. 2). However, these reactions could be considered as indirect electron dissociation of CH_4 by considering the net reactions of following reactions: $e + N_2 \rightarrow N_2^* + e$, $N_2^* + CH_4 \rightarrow$ products ($CH_x + H_y$, $x + y = 4$) + N_2. CO_2 conversion is mainly due to the reaction (R4). Note that no NOx was observed in the OES measurement.

During electron-impact dissociation reactions, many other reactive species, such as O and H atoms and OH radicals are produced. These reactive species may either facilitate further CH_4 conversion through reactions (R5–R7), or they might be consumed to produce products. As a richest carbon-containing intermediate product from the CH_4 conversion, CH_3 radicals are also important to the CH_4 conversion because it might be responsible for the CH_4 backward reaction (as R8 in R9). Regarding the products, H_2 is mainly produced from the H radical recombination and the reactions

of H with CH_4, HO_2 and HCO, whereas CO is mainly produced from electron-impact dissociation of CO_2 as well as the HCO oxidation and the reaction of HCO with CH_3 and H atoms, and hydrocarbons are produced from the recombination of CH_x (x = 1 – 3) radicals.

In our previous work [28], by independently controlling the background temperature and the reactor pressure to adjust similar reduced field intensity, we have proposed that for the CO_2/CH_4=1, the electron-induced chemistry controlled the decomposition of CH_4 and CO_2, while the rest of chemical reactions to the products were governed by thermochemistry. In this regard, the result of CO_2/CH_4=1 could be considered as a reference result to get a better understanding of the plasma chemistry with different reactant gas compositions.

In this study, at the room temperature condition, the CH_4 conversion was not influenced by the reactant compositions indicating that the CH_4 conversion was controlled by the electron-induced chemistry. It is worth mentioning that the enrichment of O atoms was observed with CO_2/CH_4=4 and O_2/CH_4=0.8 by the OES measurement as shown in Fig. 2. These enrichments could be attributed to the increased electron-impact dissociation of CO_2 for CO_2/CH_4=4 as evidenced by the higher selectivity of CO (Fig. 3b), and the effective electron-impact dissociation of O_2 for O_2/CH_4=0.8 as evidenced by the low threshold level for the electron-impact dissociation of O_2 (5.1 eV [35]) as compared to that of CO_2 (8.1 eV [36]). It seems that these enriched O atoms were not used for the CH_4 conversion at the room temperature. In contrast, at a relatively high temperature condition, the CH_4 conversion with CO_2/CH_4=4 and especially with O_2/CH_4=0.8 was enhanced as compared to that with CO_2/CH_4=1 at the similar *E/N* value. Considering the improved CH_4 conversion with CO_2/CH_4=1 at higher temperature condition was solely due to the enhanced *E/N* value [28], thermochemistry more or less affected the CH_4 conversion with CO_2/CH_4=4 and O_2/CH_4=0.8.

Figure 9a shows the reaction constants for the reactions related to CH_4 conversion under different background temperatures, where the reaction constants were obtained from [37]. The reaction constants of R5–R7 significantly increases from 5×10^{-18} to 7

$\times 10^{-14}$ cm^3 $molecule^{-1}$ s^{-1}, 7×10^{-18} to 4×10^{-13} cm^3 $molecule^{-1}$ s^{-1}, and 8×10^{-19} to 2×10^{-14} cm^3 $molecule^{-1}$ s^{-1}, respectively, in a temperature range of 293 – 673 K. Meanwhile, the CH_4 backward related reactions, R8 and R9, are not affected by the background temperature. These results indicate that at T=293 K, the low reaction constants of CH_4 conversion-related reactions contributed to the insensitive of the CH_4 conversion to the varying reactant gas composition and the CH_4 conversion is dependent of the electron-induced chemistry. At the higher temperatures, however, due to the increased reaction constants of the R5–R7, thermochemistry might control the CH_4 conversion when sufficient O containing active species (e.g. the condition of CO_2/CH_4=4, O_2/CH_4=0.8) was presented in the dry reforming process. According to our calculation using CHEMKIN-PRO package with modified USC Mech II mechanism [27, 32, 33], R6 is responsible for the enhancement of CH_4 conversion by thermochemistry at the high temperature conditions.

However, the reaction constants of H_2, CO and HCs related reactions are typically high and less sensitive to the background temperatures (Fig. 9b–9c). This led to the involvement of O containing active species in the H_2 and CO production and consumption process at all background temperatures, and thus the thermochemistry affected the products selectivity regardless of the specific background temperature. It should be noted that when O_2 was not added into the dry reforming process, CO was mostly produced from the electron-impact dissociation of CO_2 because the amount of produced CO was linearly dependent on the conversion of CO_2 as shown in Fig. S3 of the Supporting Information. Meanwhile, CO selectivity was also obviously affected by the thermochemistry because it was decreased with the background temperature. This decreased CO selectivity was accompanied by the increased HCs selectivity indicating less O containing active species was used for the CO production. We propose that the O containing active species was used in the H_2 consumption at the higher temperature condition because the reaction constants of R16 and R17 were increased with the background temperature as shown in Fig. 9c. This hypothesis is supported by the fact that the H_2 selectivity was decreased with the background temperature.

However, with the addition of O_2, CO was mainly produced from the oxidation of

HCs. This argument is supported by the evidence that the addition of O_2 had opposite effect on the CO selectivity and CO_2 conversion. According to our previous work dealing with the partial oxidation of CH_4, R18 is the major pathway for the CO production when O_2 was presented [27]. The significant consumption of carbon-based active species was also confirmed by the OES as shown in Fig. 2. Since the CH_3 was mainly used for the CO production, the low selectivity of HCs could be understood. Moreover, the addition of O_2 enriched O containing active species which lowered the selectivity of the H_2.

It is worth mentioning that with the similar reactant, the maximum conversion efficiency of CH_4 in this study was 4.9 mg/kJ, which is much less than that of CH_4 (~20 mg/kJ) with the arc-jet type plasma [38], where the arc-jet type plasma has a localized high-temperature (over several thousand kelvins [38]) environment. Our finding emphasizes that both the sufficient active species and a relatively high temperature are necessary to improve the CH_4 conversion. However, these ways to increase the CH_4 conversion also resulted in a vigorous oxidation environment which prevents the high selectivity of H_2 and HCs. Because the pathways to the products are controlled by the thermochemistry, it is possible to adjust the products distribution by controlling the reaction time of the dry reforming products. Such research is underway and will be reported in the near future.

5. Conclusions

We have investigated the dry reforming of methane to produce hydrogen and carbon monoxide in a temperature-controlled dielectric barrier discharge reactor. In particular, the performance of different CO_2/CH_4 ratios and O_2/CH_4 ratios were compared at the similar reduced field intensity to deeper understanding of the role of electron-induced chemistry and thermochemistry in the dry reforming process, where the reduced field intensity was adjusted by the background temperature. We found that at the room temperature condition, due to the low reaction constants of the reactions between CH_4 and O containing active species, the CH_4 conversion was attributed to the electron-induced chemistry rather than the thermochemistry. Two factors, relatively

high temperature and sufficient O containing active species, are necessary to make the thermochemistry important in the CH_4 conversion. In contrast, the products distribution (H_2, CO, HCs) was always controlled by the thermochemistry regardless of the specific background temperature. When the concentration of O containing active species was high, the excessive oxidation of the HCs and CO resulted in decrease of CO_2 conversion. Thus, CO_2 conversion is possibly affected by the thermochemistry even at the room temperature.

Based on the current observation, a vigorous oxidation environment is beneficial to the CH_4 conversion in the DBD reactor. The improvement of the conversion of CO_2 and the selectivity of target products (such as H_2) in such a vigorous oxidation environment is our ongoing work. Modeling works are required to fully understand the reaction pathway and to predict a way to tailor a target product.

Acknowledgment

This work was financially supported by the National Natural Science Foundation of China (No. 11775189, U1709209), and the funding from King Abdullah University of Science and Technology (BAS/1/1384-01-01).

References

[1] Aramouni N A K, Touma J G, Tarboush B A, Zeaiter J and Ahmad M N 2018 *Renew. Sust. Energ. Rev.* **82** 2570-85

[2] Wang X, Gao Y, Zhang S, Sun H, Li J and Shao T 2019 *Appl. Energy* **243** 132-44

[3] Ray D, Reddy P M K and Subrahmanyam C 2018 *Catal. Today* **309** 212-8

[4] Khoja A H, Tahir M and Amin N A S 2019 *Energ. Convers. Manage.* **183** 529-60

[5] Brune L, Ozkan A, Genty E, de Bocarmé T V and Reniers F 2018 *J. Phys. D: Appl. Phys.* **51** 234002

[6] Ray D, Nepak D, Janampelli S, Goshal P and Subrahmanyam C 2019 *Energy Technol.* **7** 1801008

[7] Wu S, Liu X, Mao W, Chen W, Liu C and Zhang C 2018 *J. Appl. Phys.* **124** 243302

[8] Wang Y, Yang H and Tu X 2019 *Energ. Convers. Manage.* **187** 593-604

[9] Wu Z, Zhou W, Hao X and Zhang X 2019 *Energy* (DOI: 10.1016/j.energy.2019.116265)

[10] Wu Z, Hao X, Zhou W, Yao S, Han J, Tang X and Zhang X 2018 *Plasma Sources Sci. Technol.* **27** 115002

[11] Zhang X and Cha M S 2016 *J. Phys. D: Appl. Phys.* **49** 175201

[12] Yao S, Weng S, Tang Y, Zhao C, Wu Z, Zhang X, Yamamoto S and Kodama S 2016 *Vacuum* **126** 16-23

[13] Wu Z, Zhu Z, Hao X, Zhou W, Han J, Tang X, Yao S and Zhang X 2018 *J. Hazard. Mater.* **347** 48-57

[14] Lian H, Liu J, Li X, Zhu X, Weber A Z and Zhu A 2019 *Chem. Eng. J.* **369** 245-52

[15] Xin Y, Sun B, Zhu X, Yan Z, Zhao X and Sun X 2018 *Int. J. Hydrogen Energy* **43** 9503-13

[16] Zhang X and Cha M S 2015 *J. Phys. D: Appl. Phys.* **48** 215201

[17] Zhang H, Wang W, Li X, Han L, Yan M, Zhong Y and Tu X 2018 *Chem. Eng. J.* **345** 67-78

[18] Rollier J, Gonzalez-Aguilar J, Petitpas G, Darmon A, Fulcheri L and Metkemeijer R 2007 *Energy Fuels* **22** 556-60

[19] Li Z, Yang T, Yuan S, Yin Y, Devid E J, Huang Q, Auerbach D and Kleyn A W 2019 *J. Energy Chem.* (DOI: 10.1016/j.jechem.2019.10.007)

[20] Tao Y, Jun S, Tangchun R, Jiao L I, Pan C and Yongxiang Y 2018 *Plasma Sources Sci. Technol.* **20** 65502

[21] Bidgoli A M, Ghorbanzadeh A, Lotfalipour R, Roustaei E and Zakavi M 2017 *Energy* **125** 705-15

[22] Wang W, Snoeckx R, Zhang X, Cha M S and Bogaerts A 2018 *J. Phys. Chem. C* **122** 8704-23

[23] Snoeckx R, Wang W, Zhang X, Cha M S and Bogaerts A 2018 *Sci. Rep.-UK* **8** 15929

[24] Sheng Z, Kameshima S, Yao S and Nozaki T 2018 *J. Phys. D: Appl. Phys.* **51** 445205

[25] Bogaerts A and Neyts E C 2018 *ACS Energy Lett.* **3** 1013-27

[26] Wang L, Yi Y, Wu C, Guo H and Tu X 2017 *Angew. Chem., Int. Ed.* **56** 13679-83

[27] Zhang X and Cha M S 2015 *P. Combust. Inst.* **35** 3447-54

[28] Zhang X and Cha M S 2013 *J. Phys. D: Appl. Phys.* **46** 415205

[29] Kogelschatz U 2003 *Plasma Chem. Plasma Process.* **23** 1-46

[30] Wagner H, Brandenburg R, Kozlov K V, Sonnenfeld A, Michel P and Behnke J F 2003 *Vacuum* **71** 417-36

[31] Zhou L M, Xue B, Kogelschatz U and Eliasson B 1998 *Energy Fuels* **12** 1191-9

[32] Wang H, You X, Joshi A V, Davis S G, Laskin A, Egolfopoulos F and Law C K 2007 http://ignis.usc.edu/USC_Mech_II.htm

[33] Seinfeld J H and Pandis S N 1998 *Atmospheric chemistry and physics: from air pollution to climate change* (New York: John Wiley & Sons) p 246-249

[34] Hagelaar G and Pitchford L C 2005 *Plasma Sources Sci. Technol.* **14** 722

[35] Chen J and Davidson J H 2003 *Plasma Chem. Plasma Process.* **23** 501-18

[36] Lee D H, Kim K, Cha M S and Song Y 2007 *P. Combust. Inst.* **31** 3343-51

[37] https://kinetics.nist.gov/ last accessed at November 5, 2019

[38] Hwang N, Song Y H, Cha M S, 2010 *IEEE Trans. Plasma Sci.* **38** 3291–3299.

Figure Caption

Figure 1. Schematic diagram of the experimental setup.

Figure 2. Typical discharge emission spectra normalized by the N_2* emission band at P_{dis} = 10 W: (a) CO_2/CH_4=1, (b) CO_2/CH_4=4, and (c) $O_2/CO_2/CH_4$=0.8:1:1.

Figure 3. Effect of CO_2/CH_4 value on the (a) CH_4, CO_2 conversion and H_2/CO, and (b) H_2, CO, C_2H_4, C_2H_6, C_3H_6, and other HCs selectivity at P_{dis} = 10 W, T=293 K.

Figure 4. Effect of O_2/CH_4 value on the dry reforming of CH_4 (a) CH_4, CO_2, O_2 conversion and H_2/CO, and (b) H_2, CO, C_2H_4, C_2H_6, C_3H_6, and other HCs selectivity at P_{dis} = 10 W, T=293 K.

Figure 5. Effect of CO_2/CH_4 value on the (a) CH_4, CO_2 conversion and H_2/CO, and (b) H_2, CO, C_2H_4, C_2H_6, C_3H_6, and other HCs selectivity at P_{dis} = 10 W, T=473 K.

Figure 6. Effect of O_2/CH_4 value on the dry reforming of CH_4 (a) CH_4, CO_2, O_2 conversion and H_2/CO, and (b) H_2, CO, C_2H_4, C_2H_6, C_3H_6, and other HCs selectivity at P_{dis} = 10 W, T=473 K.

Figure 7. Effect of *E/N* value on the dry reforming of CH_4 (a) CH_4 conversion and (b) CO_2 conversion at P_{dis} = 10 W.

Figure 8. Effect of *E/N* value on the dry reforming of CH_4 (a) H_2 selectivity, (b) CO selectivity, (c) H_2/CO, and (d) HCs selectivity at P_{dis} = 10 W.

Figure 9. Reaction constants under different reaction temperatures: (a) CH_4 conversion; (b) Competing reaction and CH_4 backward reaction; (c) H_2 production and consumption; (d) CO production and consumption.

Table 1. Summary of *E/N* values for tested conditions.

Gas composition	Absolute pressure (bar)	*T* (K)	*E/N* (Td)
CO_2/CH_4=1	1	293	70.4
		473	112.1
		573	135.8
		673	159.5
CO_2/CH_4=4	1	293	75.3
		473	118.2
		573	140.5
		673	165.2
O_2/CH_4=0.8 when CO_2/CH_4=1	1	293	80.3
		473	125.4
		573	.150.8
		673	175.1

Table 2. Important reactions related to reactant conversion and products formation

Reaction type	Reaction	Number
CH_4 and CO_2 conversion	$CH_4+e \rightarrow CH_3+H+e$	R1
	$CH_4+e \rightarrow CH_2+H_2+e$	R2
	$CH_4+e \rightarrow CH+H+H_2+e$	R3
	$CO_2+e \rightarrow CO + O$	R4
	$CH_4+O \rightarrow CH_3+OH$	R5
	$CH_4+OH \rightarrow CH_3+H_2O$	R6
	$CH_4+H \rightarrow CH_3+H_2$	R7
CH_4 backward reaction	$CH_3+H \rightarrow CH_4$	R8
	$CH_3+HCO \rightarrow CH_4+CO$	R9
Competing reaction	$CH_3+OH \rightarrow CH_3OH$	R10
	$CH_3+O \rightarrow CH_2O+H$	R11
	$CH_3+O_2 \rightarrow CH_3O_2$	R12
H_2 production	$H+H+M \rightarrow H_2+M$	R13
	$CH_4+H \rightarrow CH_3+H_2$	R7
	$H+HO_2 \rightarrow O_2+H_2$	R14
	$HCO+H \rightarrow CO+H_2$	R15
H_2 consumption	$H_2+O \rightarrow OH+H$	R16
	$H_2+OH \rightarrow H_2O+H$	R17
CO production	$HCO+O_2 \rightarrow CO+HO_2$	R18
	$HCO+OH \rightarrow CO+H_2O$	R19
	$HCO+O \rightarrow CO+OH$	R20
	$CH_3+HCO \rightarrow CH_4+CO$	R9
	$HCO+H \rightarrow CO+H_2$	R15
CO consumption	$CO+O \rightarrow CO_2$	R21
	$CO+OH \rightarrow CO_2+H$	R22
	$HO_2+CO \rightarrow OH+CO_2$	R23

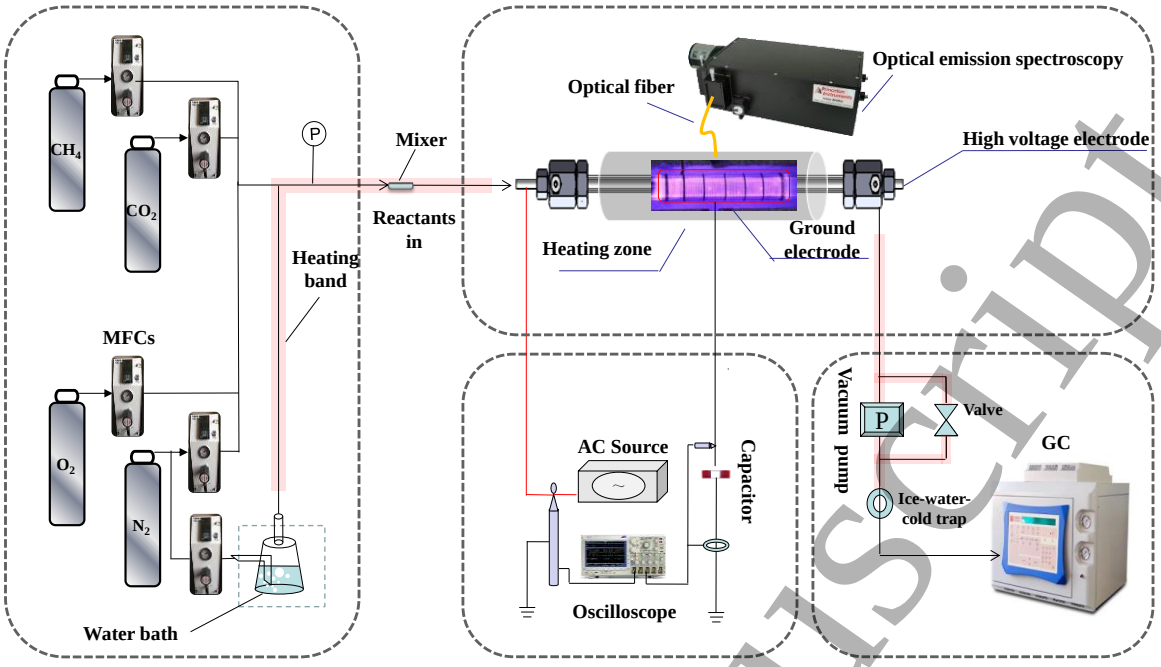

Figure 1. Schematic diagram of the experimental setup.

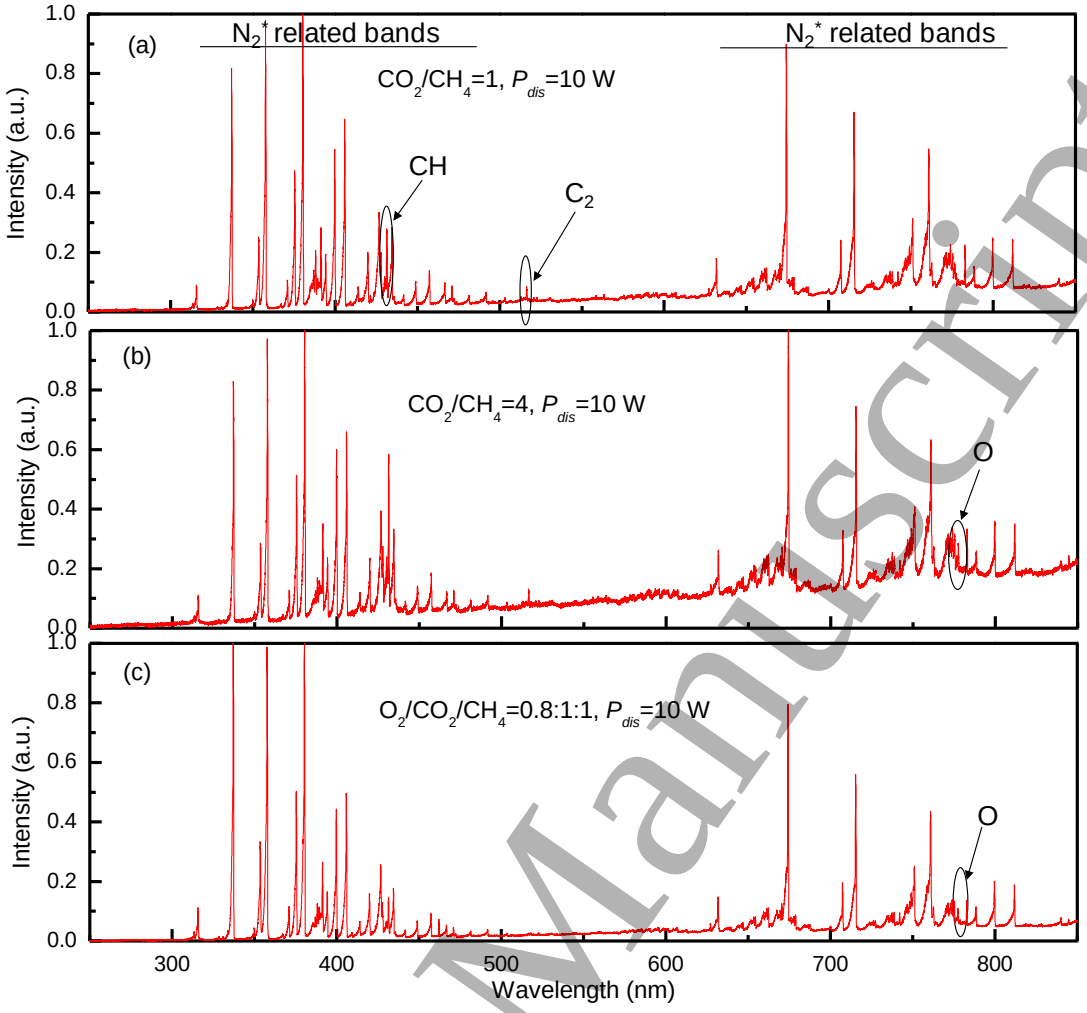

Figure 2. Typical discharge emission spectra normalized by the N_2* emission band at P_{dis} = 10 W: (a) CO_2/CH_4=1, (b) CO_2/CH_4=4, and (c) $O_2/CO_2/CH_4$=0.8:1:1.

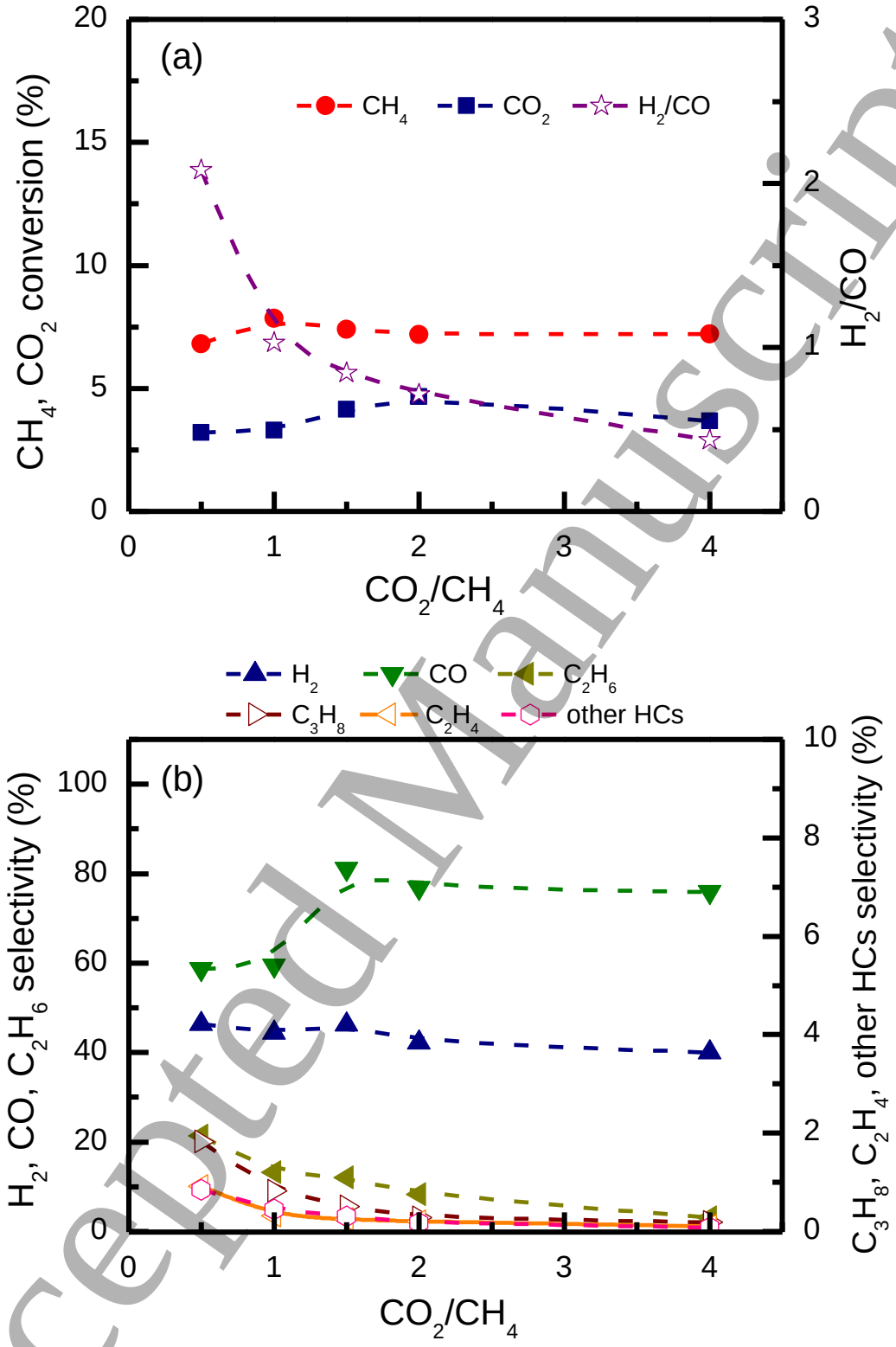

Figure 3. Effect of CO_2/CH_4 value on the (a) CH_4, CO_2 conversion and H_2/CO, and (b) H_2, CO, C_2H_4, C_2H_6, C_3H_6, and other HCs selectivity at P_{dis} = 10 W, T=293 K.

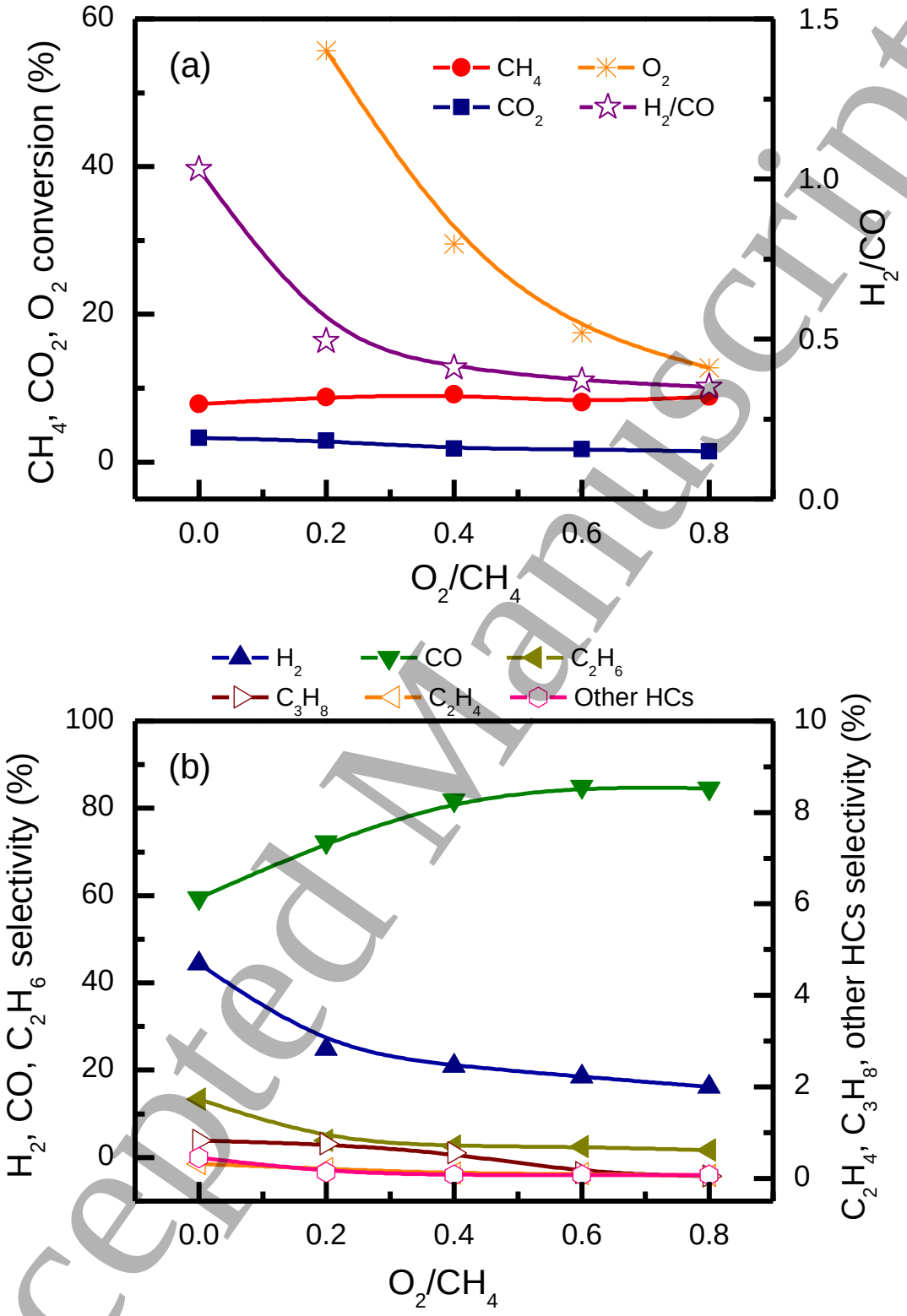

Figure 4. Effect of O_2/CH_4 value on the dry reforming of CH_4 (a) CH_4, CO_2, O_2 conversion and H_2/CO, and (b) H_2, CO, C_2H_4, C_2H_6, C_3H_6, and other HCs selectivity at P_{dis} = 10 W, T=293 K.

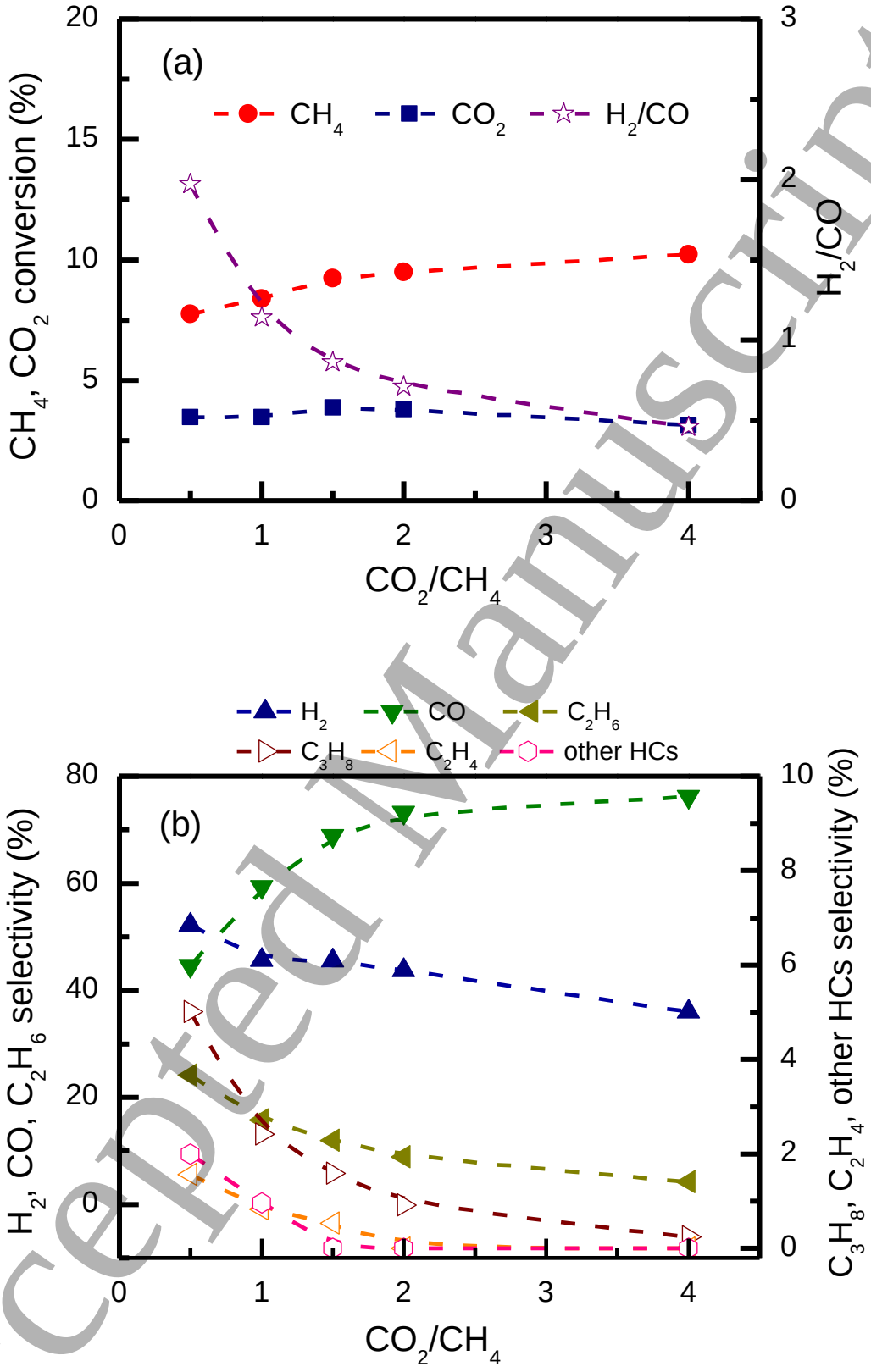

Figure 5. Effect of CO_2/CH_4 value on the (a) CH_4, CO_2 conversion and H_2/CO, and (b) H_2, CO, C_2H_4, C_2H_6, C_3H_6, and other HCs selectivity at P_{dis} = 10 W, T=473 K.

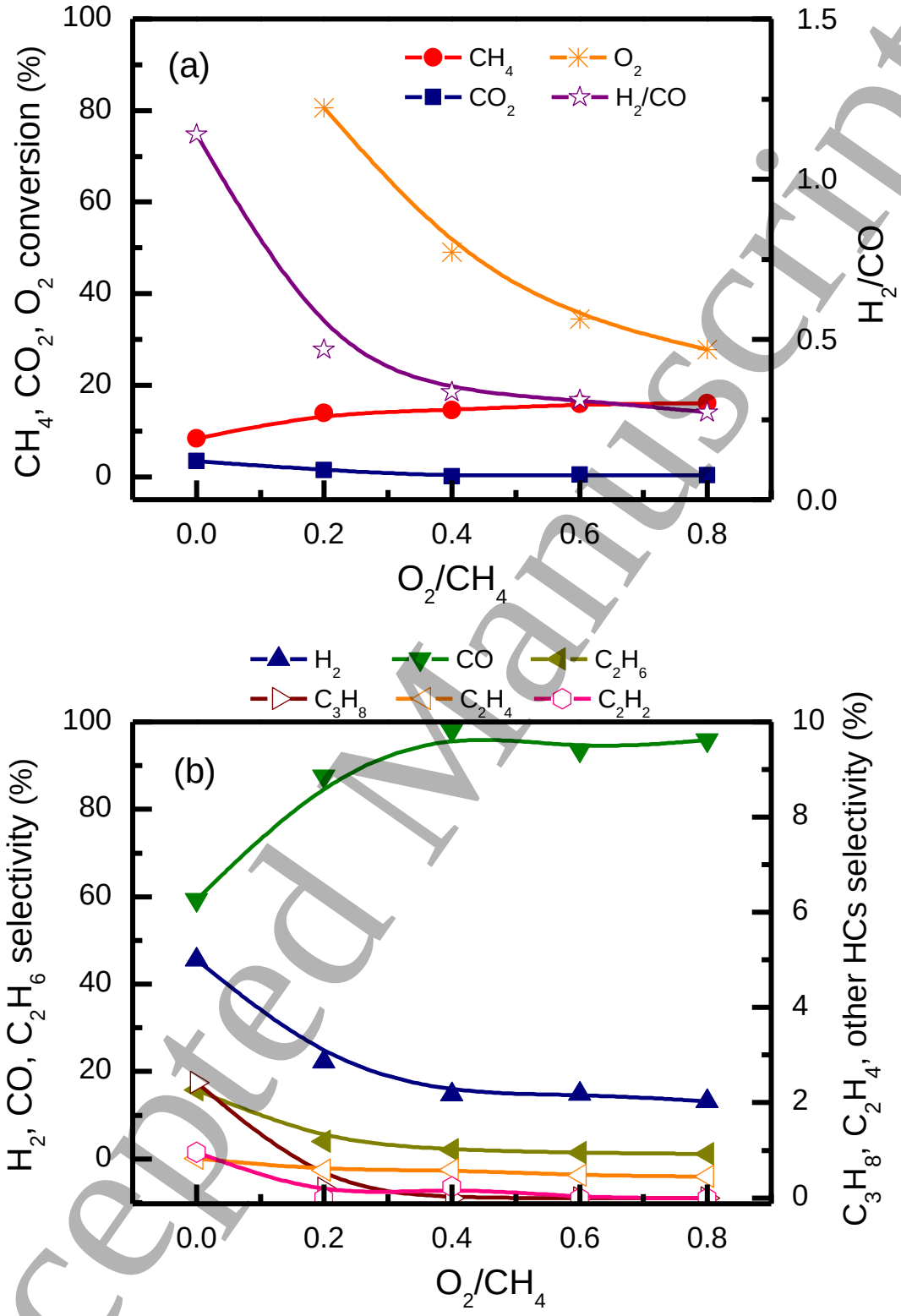

Figure 6. Effect of O_2/CH_4 value on the dry reforming of CH_4 (a) CH_4, CO_2, O_2 conversion and H_2/CO, and (b) H_2, CO, C_2H_4, C_2H_6, C_3H_6, and other HCs selectivity at

P_{dis} = 10 W, T=473 K.

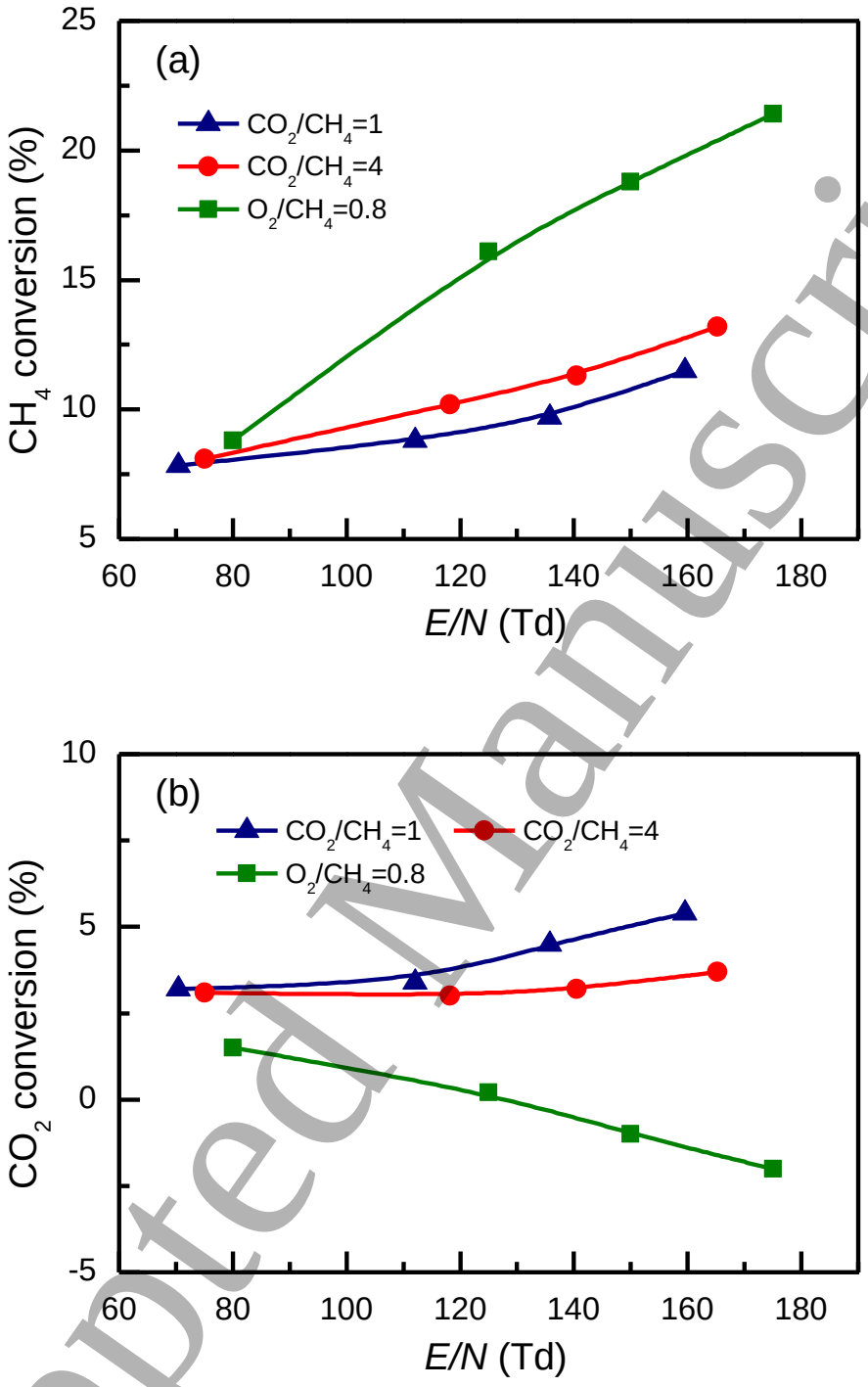

Figure 7. Effect of *E/N* value on the dry reforming of CH_4 (a) CH_4 conversion and (b) CO_2 conversion at P_{dis} = 10 W.

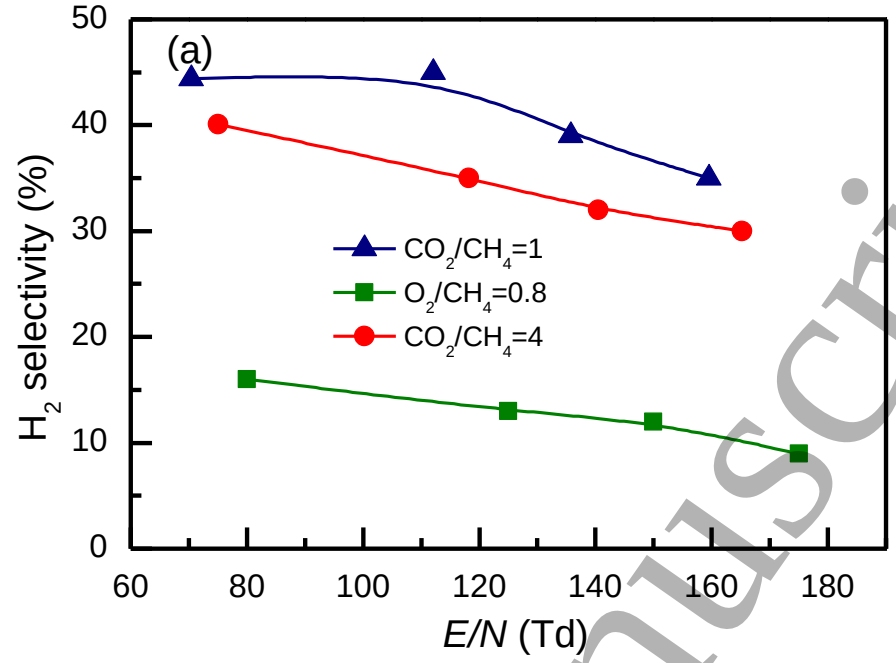

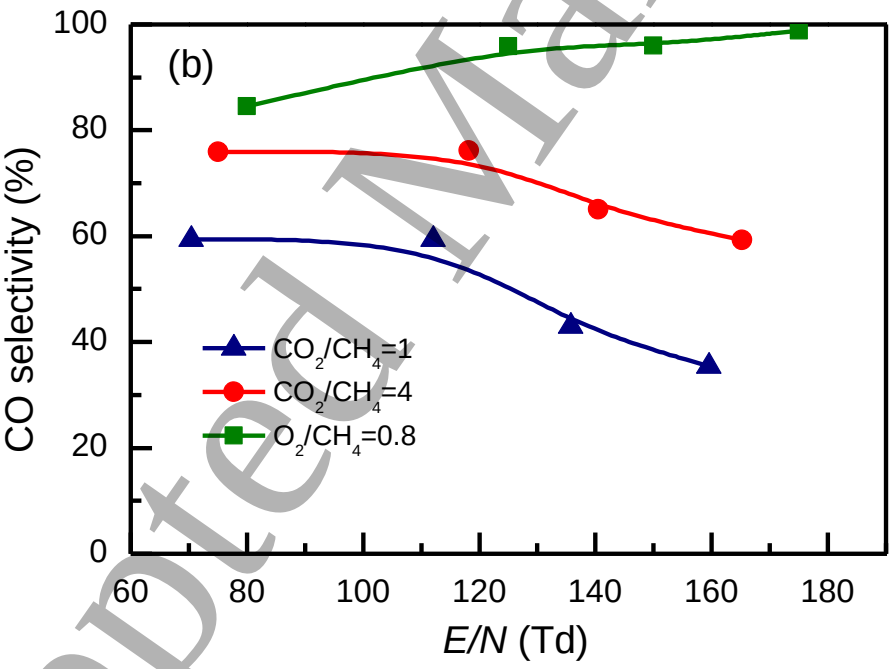

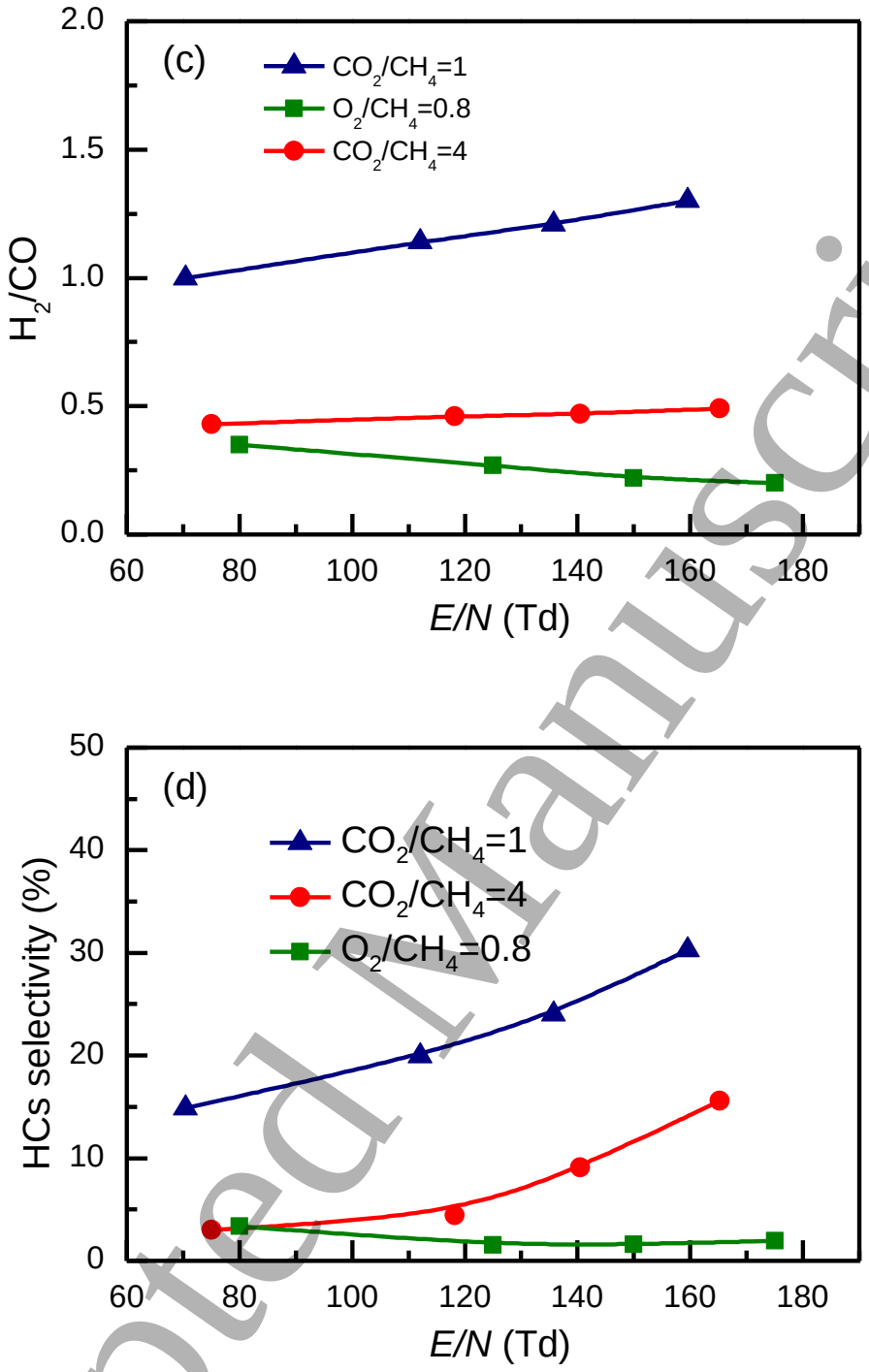

Figure 8. Effect of *E/N* value on the dry reforming of CH_4 (a) H_2 selectivity, (b) CO selectivity, (c) H_2/CO, and (d) HCs selectivity at P_{dis} = 10 W.

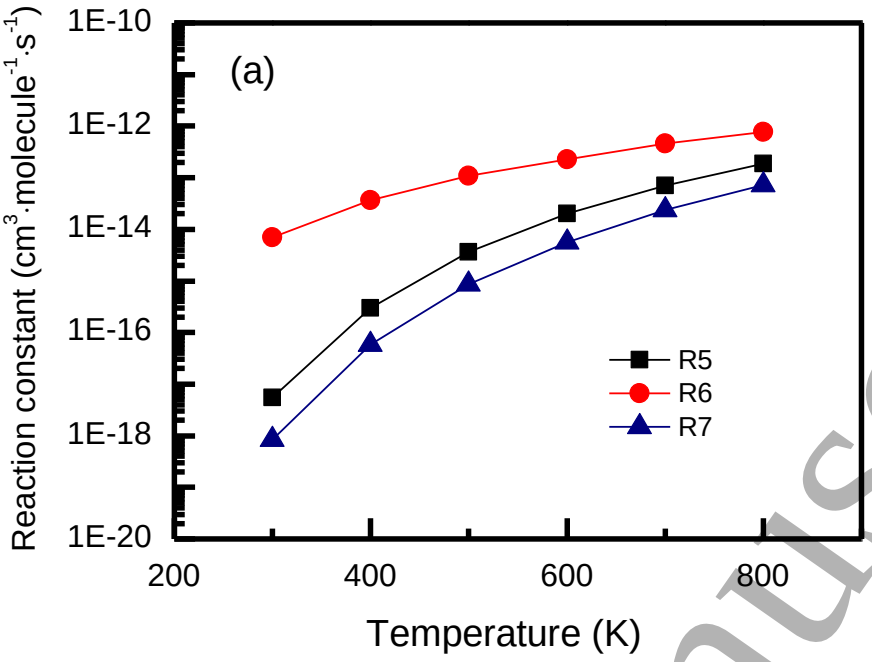

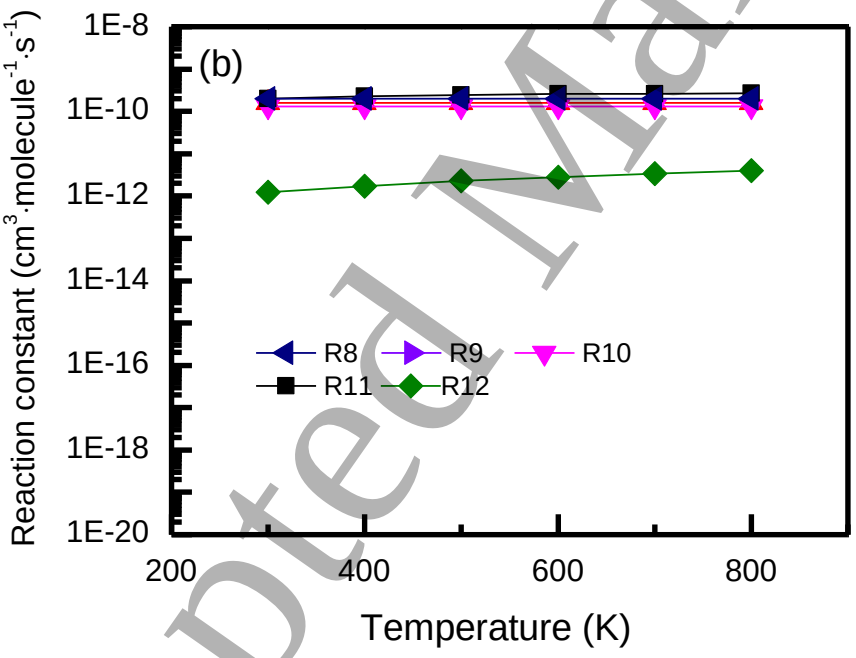

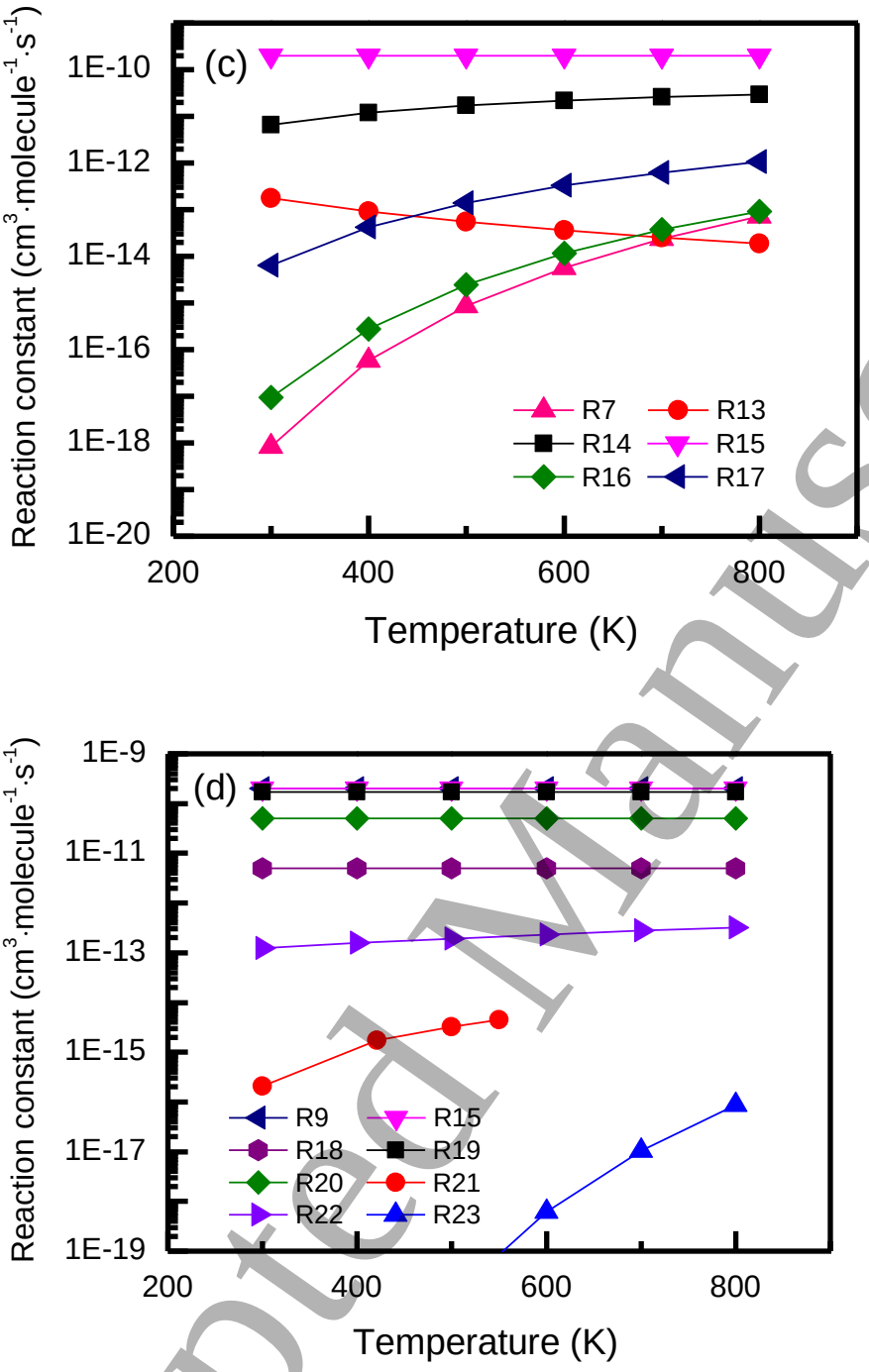

Figure 9. Reaction constants under different reaction temperatures: (a) CH_4 conversion; (b) Competing reaction and CH_4 backward reaction; (c) H_2 production and consumption; (d) CO production and consumption.